Monte Carlo-based inverse model for calculating tissue optical properties. Part II: Application to breast cancer diagnosis

Gregory M. Palmer, Changfang Zhu, Tara M. Breslin, Fushen Xu, Kennedy W. Gilchrist, and Nirmala Ramanujam

The Monte Carlo-based inverse model of diffuse reflectance described in part I of this pair of companion papers was applied to the diffuse reflectance spectra of a set of 17 malignant and 24 normal–benign *ex vivo* human breast tissue samples. This model allows extraction of physically meaningful tissue parameters, which include the concentration of absorbers and the size and density of scatterers present in tissue. It was assumed that intrinsic absorption could be attributed to oxygenated and deoxygenated hemoglobin and beta-carotene, that scattering could be modeled by spheres of a uniform size distribution, and that the refractive indices of the spheres and the surrounding medium are known. The tissue diffuse reflectance spectra were evaluated over a wavelength range of 400–600 nm. The extracted parameters that showed the statistically most significant differences between malignant and nonmalignant breast tissues were hemoglobin saturation and the mean reduced scattering coefficient. Malignant tissues showed decreased hemoglobin saturation and an increased mean reduced scattering coefficient compared with nonmalignant tissues. A support vector machine classification algorithm was then used to classify a sample as malignant or nonmalignant based on these two extracted parameters and produced a cross-validated sensitivity and specificity of 82% and 92%, respectively.

OCIS codes: 170.4580, 170.6510, 160.4760.

1. Introduction

Diffuse reflectance spectroscopy in the ultraviolet–visible (UV–VIS) wavelength range can be used to measure tissue absorption and scattering, which reflect the intrinsic physiological and structural properties of tissue. This technique has the potential to provide real-time, nondestructive, and quantitative means of characterizing tissue pathology. It thus presents an opportunity to fill a void in postscreening cancer care, in which currently a biopsy is typically required for providing a definitive diagnosis. For example, in the case of breast cancer diagnosis, an image-guided needle biopsy procedure is commonly performed to determine whether a lesion is cancerous in women with suspicious mammograms. However, such procedures are limited in that only a few small pieces of tissue can be removed. Additionally, the tissue must be fixed and read by a pathologist before a diagnosis can be made, often requiring a waiting period of several days to weeks. The limited sampling yield of breast needle biopsy results in a false-negative rate of 1%–7% (Ref. 1) when verified with follow-up mammography, as well as the requirement for repeat biopsies (percutaneous or surgical) in 9%–18% of patients[2,3] because of discordance between histological findings and mammography. Diffuse reflectance spectroscopy has the potential to improve the sampling accuracy of breast core needle biopsy. This technology could be deployed through fiber-optic probes to quickly and nondestructively identify the tissue type (normal, benign, or malignant) at the needle tip during a breast biopsy procedure. A positive reading from the optical measurement would potentially increase the likelihood that a biopsy is being sampled from a tumor site. If the optical measurement reads negative, then the

G. M. Palmer and N. Ramanujam (nimmi@duke.edu) are with the Department of Biomedical Engineering, 136 Hudson Hall, Box 90281, Duke University, Durham, North Carolina 27708-0281. C. Zhu is with the Department of Electrical and Computer Engineering, University of Wisconsin, Madison, Wisconsin. T. M. Breslin is with the Department of Surgery, University of Wisconsin, Madison, Wisconsin. F. Xu and K. W. Gilchrist are with the Department of Pathology, University of Wisconsin, Madison, Wisconsin.

Received 29 March 2005; accepted 15 July 2005.
0003-6935/06/051072-07$15.00/0

needle could be repositioned along the needle track to a new tissue site. Diffuse reflectance spectroscopy techniques could potentially make the breast biopsy procedure more accurate and less traumatic to the patient, while also reducing the number of biopsies that need to be processed to obtain a confirmatory diagnosis.

Previous studies have investigated the use of diffuse reflectance spectroscopy for the diagnosis of breast cancer. The majority of these studies have utilized empirical methods for analysis of the measured spectra (e.g., Refs. 4–6). Empirical techniques are limited in that they do not relate the measured spectra to physically meaningful information (the absorption and scattering properties of the tissue). Doing so may improve our understanding of the basis under which the diagnosis is made, as well as potentially improving the diagnostic accuracy.

Ghosh *et al.*[7] used a model based on the standard diffusion approximation to extract the absorption and scattering coefficients from spatially resolved diffuse reflectance measurements of human breast tissue samples. They measured the spatially resolved diffuse reflectance at 12 source–detector separations, ranging from 1.2 to 12 mm, over the wavelength range of 450–650 nm. The absorption and scattering coefficients were determined from fits to the diffusion approximation of the spatially resolved diffuse reflectance at each individual wavelength. The results from this analysis indicated that malignant tissues are more absorbing and scattering than normal tissues at all wavelengths. However, limitations of the analysis used in this study include the use of the diffusion approximation, which is valid only for cases in which absorption is much lower than scattering (this may not be a valid assumption in the UV–VIS spectral range), and the requirement for spatially resolved measurements.

To address these concerns, the inverse Monte Carlo-based model developed by our group is valid for a wide range of optical properties and for diffuse reflectance measurements that are not spatially resolved, provided a single phantom calibration measurement is made (described in the companion paper, part I.[8] In this paper, this model is applied to a set of diffuse reflectance spectra obtained from *ex vivo* breast tissues collected in a previous study.[4] In the previous study, the diffuse reflectance spectra were analyzed by use of empirical methods. The objectives of this study are to (1) analyze the diffuse reflectance spectra of the breast tissues by use of the Monte Carlo model, (2) evaluate the absorption and scattering properties that contribute to the diagnosis of breast cancer, and (3) directly compare the diagnostic accuracy of the Monte Carlo versus empirically based methods developed by our group.

2. Methods

A. Spectral Data Collected from Breast Tissue Samples

Diffuse reflectance spectra were collected from 41 human breast tissues taken from 23 women undergoing breast cancer or breast reduction surgery. There were a total of 17 malignant tissue samples, 6 normal and 4 benign fibrous–glandular tissues, and 14 adipose tissues, as determined by the gold standard, histopathology. These spectra were obtained in a previous study[4] with the same instrument and probe described in part I of this study.[8] Measurements were made on freshly excised tissue samples, within approximately 2 h of excision, by placing the probe in light contact with the tissue surface.

B. Data Analysis

Model description. A Monte Carlo-based inverse model was used to extract the absorption and scattering parameters from the measured diffuse reflectance spectra; this model is described in detail in part I of this pair of companion papers.[8] The fixed parameters of the model were the absorbers assumed to be present in the tissue, the extinction coefficient of the absorbers, and the refractive index mismatch between the scatterer and the surrounding medium. The free parameters of the model were the concentration of absorbers and the scatterer size and density. A nonlinear least-squares optimization algorithm minimized the difference between the modeled and the measured diffuse reflectance spectra, and the free parameters of the best fit were retained for further analysis.

Wavelength range used in the model. The diffuse reflectance spectra of the breast tissues were measured over the wavelength range of 300–700 nm in 5 nm increments. However, the diffuse reflectance spectra analyzed by the inverse model were restricted to the wavelength range of 400–600 nm. The wavelength range was restricted to simplify the use of the model in this initial study by reducing the number of absorbers that would have to be accounted for (by excluding proteins and other chromophores that absorb below 400 nm) and to ensure that the tissue could be modeled as a semi-infinite medium (by excluding wavelengths above 600 nm, where tissue has very low absorption). The semi-infinite assumption simplifies the model since the depth does not also need to be fit as a free parameter. The tissue samples, which were 3 mm or greater in thickness, were found to be too thin to be modeled as semi-infinite at wavelengths greater than 600 nm. We determined experimentally by placing a reflective and absorptive surface beneath the sample during the diffuse reflectance measurement.

Calibration for system response. Before the fitting, each tissue diffuse reflectance spectrum was divided at each wavelength by the diffuse reflectance spectrum of a reference tissue phantom composed of hemoglobin and polystyrene spheres with known optical properties (mean reduced scattering coefficient μ_s', 13 cm^{-1}; mean absorption coefficient μ_a, 0.9 cm^{-1}). We calibrated the modeled diffuse reflectance spectra in a similar manner, i.e., by dividing the modeled diffuse reflectance spectra by that of a reference phantom with the same predefined optical

properties. This accounted for the throughput and the wavelength response of the spectrometer used in these studies and corrected differences in magnitude between the Monte Carlo simulations, which are on an absolute scale, and the experimental measurements, which are on a relative scale.

Fixed and free parameters used in the model. The inverse model assumes scattering to be caused by spherical scatterers of a single size. Tissue would be expected to contain scatterers of a range of sizes and shapes. However, the single-sized spherical approximation was chosen to allow a simpler solution and produce a composite description of scattering. The effect of using only a single scatterer size was investigated in part I and was found to have a minimal effect on the accuracy of optical property extraction.[8] The refractive indices of the scatterers and the surrounding medium were fixed parameters and were assumed to be 1.4 and 1.36, respectively. The free parameters of the fit relating to scattering were scatterer size and density. The scatterer size was constrained to be between 0.35 and 1.5 μm in diameter.[9–13] The intrinsic chromophores were assumed to be oxygenated and deoxygenated hemoglobin and beta-carotene,[4,14] and their wavelength-dependent extinction coefficients were obtained from an on-line database.[15] Lymphazurin (cat. no. 00592358, Tyco Healthcare, Mansfield, Massachusetts), a dye used to locate the sentinel lymph node during surgery, was also included as an absorber since it was found to be present in some of the tissue samples. Its wavelength-dependent extinction coefficient was measured with a spectrophotometer. The free parameters of the fit relating to absorption were the concentrations of each absorber. Note that the Lymphazurin concentration was not used in the classification algorithm; thus only intrinsic sources of contrast were used.

Diagnosis of breast cancer using the extracted parameters. After the inverse model was applied to the diffuse reflectance spectra to extract the absorption and scattering parameters, a Wilcoxon rank-sum test[16] was used to determine which extracted features showed statistically significant differences between malignant and nonmalignant breast tissues. Then, a previously developed[4] nonparametric, linear support vector machine (SVM) algorithm[17,18] was adapted to classify each tissue sample based on these extracted features. Finally, an unbiased estimate of the algorithm's performance was carried out with the leave-one-out method in this study.[19]

3. Results

Figure 1 shows the diffuse reflectance spectra of a malignant [Fig. 1(a)] and an adipose breast tissue sample [Fig. 1(b)] obtained from the same patient and the corresponding fit to the inverse Monte Carlo model. Two different fits were carried out. The first fit included the four absorbers: oxygenated hemoglobin, deoxygenated hemoglobin, beta-carotene, and Lymphazurin (fitted). It should be pointed out that when only the four absorbers are used in the fit, a

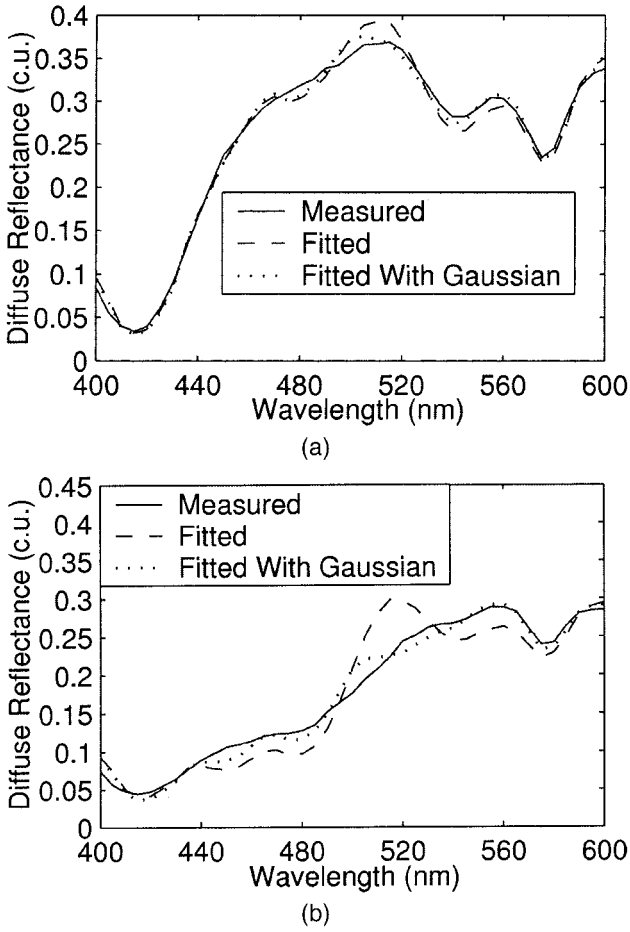

Fig. 1. Diffuse reflectance spectra of (a) a malignant and (b) an adipose breast tissue sample obtained from the same patient and the corresponding fit to the inverse Monte Carlo model. Two different fits were carried out. The first fit included the four absorbers: oxygenated hemoglobin, deoxygenated hemoglobin, beta-carotene, and Lymphazurin (fitted). The second fit included the same four absorbers and an additional Gaussian function (fitted with Gaussian). c.u., calibrated units.

deviation from the measured spectra is present at ~500–530 nm. This deviation was present in fits to the diffuse reflectance spectra of a number of tissue samples and likely indicates a region where the absorbers present in the tissue are not well described by the inverse model. To further evaluate this possibility, a Gaussian function was included as an additional absorbing component in the fit to the inverse model. The mean of the function was fixed at 515 nm, whereas the standard deviation and magnitude of the Gaussian were set as free parameters. The second fit seen in the plot included the four absorbers and an additional Gaussian function (fitted with Gaussian). It can be seen that the addition of this Gaussian function substantially improves the quality of the fits. Furthermore, for the majority of the fits (33 out of 41), the Gaussian function was found to have a standard deviation between 9 and 16 nm, with an average value of 13 nm. Repeating the fits to the inverse model with a Gaussian function with a mean

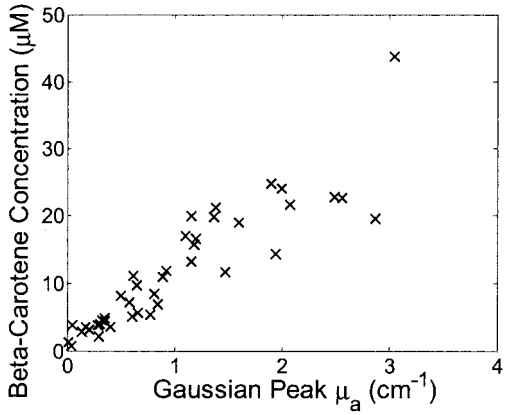

Fig. 2. Scatter plot of the beta-carotene concentration and peak μ_a of the Gaussian absorber. It can be seen that these two parameters are highly correlated (the correlation coefficient is 0.9).

of 515 nm and a standard deviation of 13 nm produced a similar improvement in the quality of the fits. As seen in Fig. 2, the peak absorption coefficient of the Gaussian function is highly correlated with the concentration of beta-carotene, with a Pearson's correlation coefficient of 0.9. Although the quality of the fits is improved with the addition of the Gaussian function, the conclusions regarding the extracted absorber and scattering parameters from the fits are not significantly affected by its addition, and so all subsequent analysis was carried out without the inclusion of this Gaussian function.

The same malignant and adipose tissue samples shown in Fig. 1 (obtained without the Gaussian function) are shown in Fig. 3 with the extracted absorption [Fig. 3(a)] and reduced scattering coefficient spectra [Fig. 3(b)] extracted from their fits. These are fits to single tissue samples, representative of their respective tissue types. It can be seen that both samples have significant hemoglobin absorption, whose peak absorption occurs at approximately 420 nm, and that the malignant sample shows higher hemoglobin absorption compared with that in adipose tissue. Additionally, it can be seen that the adipose tissue sample has a distinctly different line shape in the absorption spectrum, particularly over the wavelength range of 450–500 nm. The absorption in this range is in part due to beta-carotene in adipose tissues. It can also be seen that the reduced scattering coefficient is substantially reduced in the adipose tissue compared with that in the malignant tissue.

Figure 4 shows the mean and standard deviations of the extracted hemoglobin and beta-carotene concentrations [Fig. 4(a)], hemoglobin saturation [Fig. 4(b)], and mean μ_s' (averaged over the 400–600 nm wavelength range) [Fig. 4(c)] of adipose, fibrous, and malignant breast tissues. In these plots, it can be seen that adipose tissues have higher hemoglobin saturation ($p < 10^{-4}$, obtained with a Wilcoxon rank-sum test) and beta-carotene concentration ($p < 0.001$) and a lower mean μ_s' ($p < 10^{-4}$) compared with malignant tissues. Fibrous tissues can

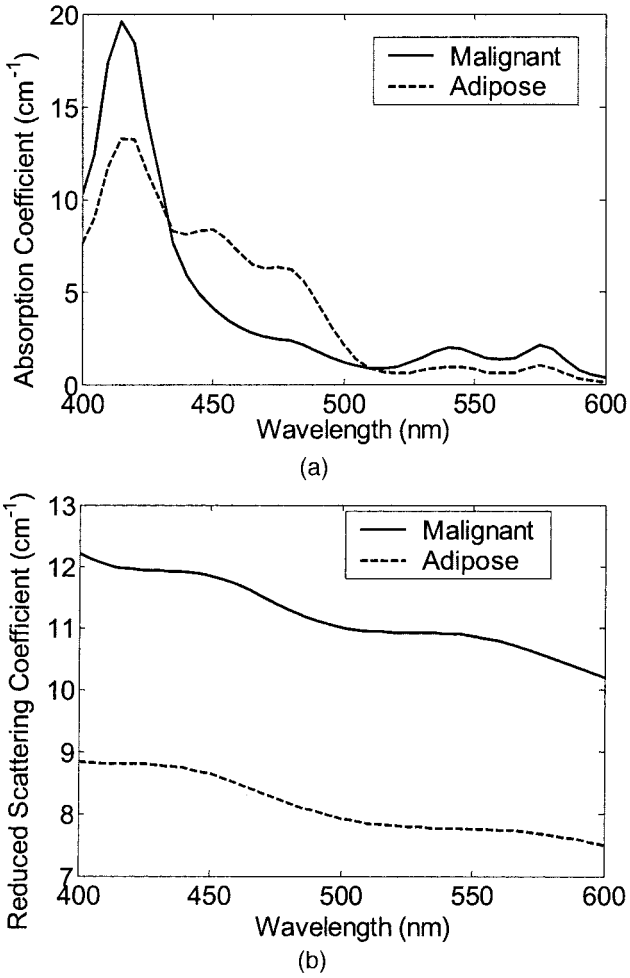

Fig. 3. Extracted (a) absorption coefficient and (b) reduced scattering coefficient spectra extracted from the fits to the malignant and adipose tissue diffuse reflectance spectra (obtained without the Gaussian function).

also be seen to have a higher hemoglobin saturation ($p < 0.005$) compared with that in malignant tissues. In comparing the malignant with the collective nonmalignant tissue types (adipose and fibrous–glandular tissues), three extracted parameters were found to show significant differences. Hemoglobin saturation ($p < 10^{-5}$) and beta-carotene concentration ($p < 0.05$) were significantly decreased, and the mean μ_s' ($p < 0.05$) was significantly increased in malignant tissues compared with that in the collective nonmalignant tissue types. To summarize, differences seen in beta-carotene and mean μ_s' are primarily due to differences between adipose and malignant tissues, whereas hemoglobin saturation is useful in distinguishing malignant from both fibrous–glandular and adipose tissues. It should be pointed out that, in the case in which a Gaussian absorber is included in the fits, the same parameters show statistically significant differences between malignant and nonmalignant tissues, with the exception of beta-carotene concentration, which has a p value of 0.025 in the case in which no Gaussian function is

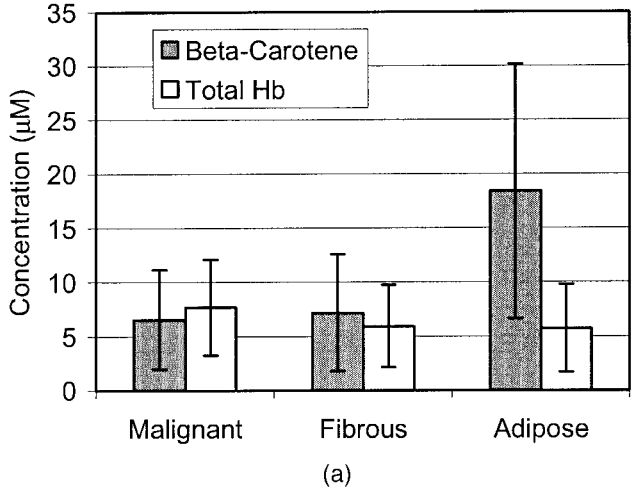

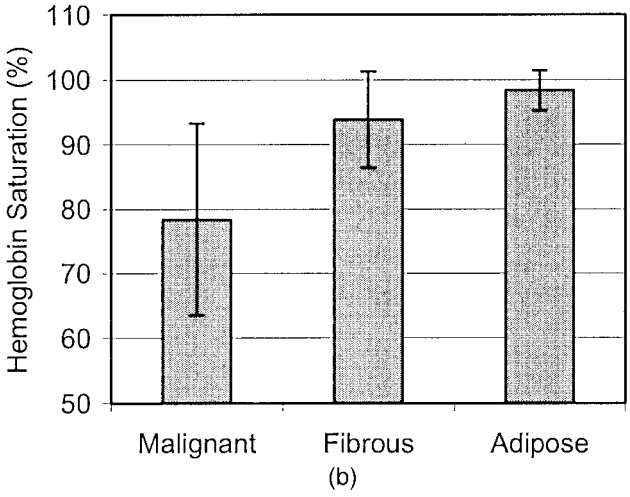

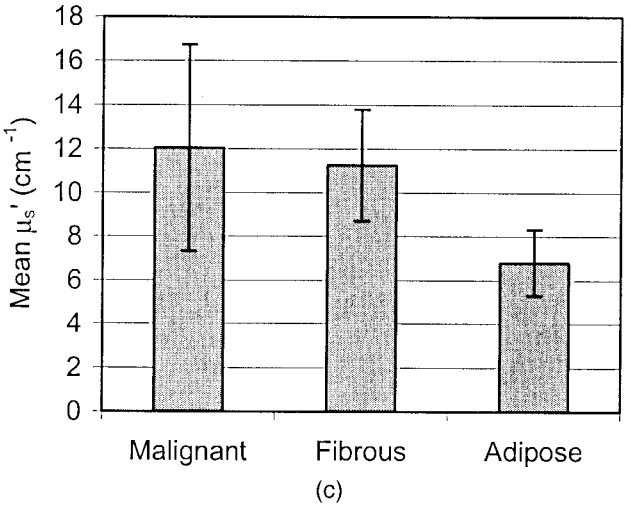

Fig. 4. Mean and standard deviations of (a) hemoglobin and beta-carotene concentrations, (b) hemoglobin saturation, and (c) mean μ_s' averaged over the wavelength range of 400–600 nm of adipose, fibrous, and malignant breast tissues. The most significant differences between malignant and nonmalignant tissue are seen in hemoglobin saturation, beta-carotene concentration, and the mean μ_s'. Note that a fibrous sample with an extracted total hemoglobin concentration of 87 μM was excluded from plot (a) since it drastically skewed the plot scale.

included, and a p value of 0.093 in the case in which a Gaussian function is included. However, when malignant and adipose tissues are compared, the difference in beta-carotene concentration is still highly significant ($p < 5 \times 10^{-4}$).

Figure 5 shows a scatter plot of two extracted parameters, hemoglobin saturation and the reduced scattering coefficient, which showed the statistically most significant differences between malignant and nonmalignant breast tissues. The discrimination boundary from the linear SVM algorithm that separates the malignant from nonmalignant tissues is also shown. It can be seen that good separation can be achieved between the malignant and nonmalignant tissue types with only these two extracted parameters. The classification accuracy (sensitivity and specificity) for discriminating between malignant and nonmalignant breast tissues was determined with the linear SVM algorithm based on these two extracted features. A cross-validation scheme was used to provide an unbiased estimate of the algorithm's performance. The unbiased sensitivity and specificity of the algorithm were 82% and 92%, respectively. We define sensitivity as the number of correctly classified malignant samples divided by the total number of malignant samples, and specificity is the number of correctly classified nonmalignant samples divided by the total number of nonmalignant samples.

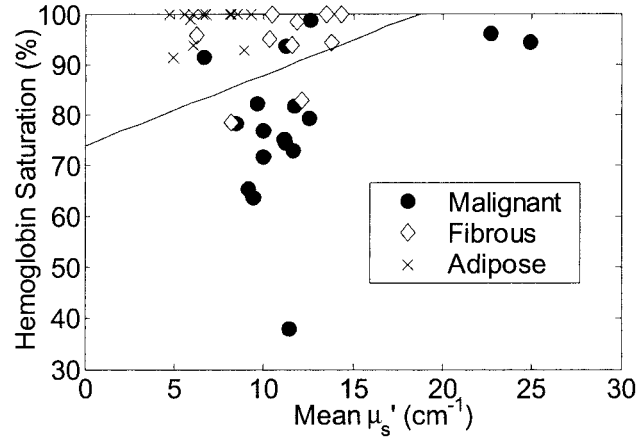

Fig. 5. Scatter plot of two extracted parameters, hemoglobin saturation and mean μ_s', which showed the statistically most significant differences between malignant and nonmalignant breast tissues.

4. Discussion and Conclusions

A Monte Carlo-based inverse model of diffuse reflectance, described in part I of this pair of companion papers, was applied to the diffuse reflectance spectra of a set of 17 malignant and 24 normal–benign *ex vivo* human breast tissue samples. This model allows extraction of physically meaningful tissue parameters, which include the concentration of absorbers and the mean reduced scattering coefficient that reflects the size and density of scatterers present in tissue. The parameters that showed the statistically most significant differences between malignant and nonmalignant tissues included hemoglobin saturation, beta-carotene concentration, and the mean reduced scattering coefficient. When broken down by tissue type, hemoglobin saturation was found to be useful in distinguishing malignant from both fibrous–glandular and adipose tissues, whereas beta-carotene concentration and the mean reduced scattering coefficient were useful in distinguishing malignant from adipose tissue only. A linear SVM algorithm,[17,18] incorporating two of the three parameters (hemoglobin saturation and mean μ_s'), yielded a sensitivity and specificity of 82% and 92%, respectively, for discriminating between malignant and nonmalignant breast tissues when a leave-one-out cross-validation scheme is used. In a previous publication by our group,[4] a principal-component analysis[20] was used to dimensionally reduce the same set of breast tissue diffuse reflectance spectra into a few orthogonal principal components; a Wilcoxon rank-sum test[16] was applied to identify the two principal components that showed the statistically most significant differences between malignant and nonmalignant breast tissues, and a linear SVM algorithm[18] was used as the classification scheme. An unbiased evaluation of the algorithm's performance was performed with a leave-one-out cross-validation method.[19] The previously published algorithm produced a sensitivity and specificity of 30% and 77%, respectively, for discriminating between malignant and nonmalignant breast tissues. The only difference between the previously published algorithm and the algorithm reported in this paper is the method of data reduction (principal-component analysis versus fits to an inverse Monte Carlo model). This demonstrates that the physically based approach for data reduction substantially outperforms the empirically based algorithm implemented previously. However, it is possible that the use of other empirically based algorithms such as the partial least-squares techniques[21] could improve on this result.

Hemoglobin saturation showed a significant decrease in malignant tissue relative to that of each of the nonmalignant tissue types. This trend is consistent with previous findings obtained from near-infrared (NIR) measurements of breast tissues *in vivo*.[22–25] These studies compared the hemoglobin saturation of a malignant lesion with that of the surrounding normal tissues (either adipose or fibrous–glandular) and found that there is a decrease in the hemoglobin saturation in the volume comprising the lesion. No significant difference in the total hemoglobin concentration between malignant and nonmalignant breast tissues was observed in our study as would be expected with angiogenesis and which has also been reported in several previous NIR studies of the breast *in vivo*.[22–27] It should be pointed out that the oxygen saturation values for adipose and fibrous tissues were typically above 90%, which is higher than would be expected in excised tissue. It is possible that this result is affected by exposure to air of residual blood on or near the surface of the tissue, which would cause an increase in the saturation levels. The sample thickness was typically 3 mm or greater, so some blood would also likely be detected from deeper within the tissue that was not exposed to air. The greater vascularity expected in malignant tissue may have led to more residual blood trapped deep within the tissue, which could have resulted in the lower saturation detected in these tissues. Finally, our study showed that the mean reduced scattering coefficient is higher in malignant tissues compared with that in adipose tissues. This is consistent with that reported from NIR measurements of breast tissues *in vivo* by Srinivasan *et al.*[28]

One limitation of this model is that it requires *a priori* knowledge of the absorbers and scatterers present in the tissue of interest. For many tissue types, hemoglobin is the primary absorber in the VIS wavelength range. In adipose breast tissue, beta-carotene has also been observed to cause significant absorption effects,[4,14] and so it was included. It was pointed out that there was a systematic deviation in the fits to the diffuse reflectance spectra at ~500–530 nm, which could be corrected for by the inclusion of a Gaussian function. The contribution of this Gaussian function to the fitted spectrum was highly correlated with the concentration of beta-carotene. Thus the Gaussian function effectively modified the spectral shape of the absorption spectrum of beta-carotene. This implies that the beta-carotene absorption spectrum utilized in these fits may not accurately reflect that present in human breast tissues, possibly as a result of differences in its surrounding environment in tissue. It is also possible that the combination of beta-carotene and the Gaussian represent a different absorber. However, the inclusion of the Gaussian function, although it improved the quality of the fits, did not affect the extracted parameters that showed the statistically most significant differences between malignant and nonmalignant breast tissues.

This work was funded by University of Wisconsin Radiological Sciences Training grant 5T32CA009206-27, sponsored by the National Institutes of Health, the Department of Health and Human Services, and the Public Health Service. Additional funding was provided by the National Institutes of Health through grant 1R01CA100559-01A1.

References

1. R. J. Jackman, K. W. Nowels, J. Rodriguez-Soto, F. A. Marzoni, Jr., S. I. Finkelstein, and M. J. Shepard, "Stereotactic, auto-

mated, large-core needle biopsy of nonpalpable breast lesions: false-negative and histologic underestimation rates after long-term follow-up," Radiology **210,** 799–805 (1999).
2. D. D. Dershaw, E. A. Morris, L. Liberman, and A. F. Abramson, "Nondiagnostic stereotaxic core breast biopsy: results of rebiopsy," Radiology **198,** 323–325 (1996).
3. J. E. Meyer, D. N. Smith, S. C. Lester, P. J. DiPiro, C. M. Denison, S. C. Harvey, R. L. Christian, A. Richardson, and W. D. Ko, "Large-needle core biopsy: nonmalignant breast abnormalities evaluated with surgical excision or repeat core biopsy," Radiology **206,** 717–720 (1998).
4. G. M. Palmer, C. Zhu, T. M. Breslin, F. Xu, K. W. Gilchrist, and N. Ramanujam, "Comparison of multiexcitation fluorescence and diffuse reflectance spectroscopy for the diagnosis of breast cancer," IEEE Trans. Biomed. Eng. **50,** 1233–1242 (2003).
5. I. J. Bigio, S. G. Bown, G. Briggs, C. Kelley, S. Lakhani, D. Pickard, P. M. Ripley, I. G. Rose, and C. Saunders, "Diagnosis of breast cancer using elastic-scattering spectroscopy: preliminary clinical results," J. Biomed. Opt. **5,** 221–228 (2000).
6. Y. Yang, E. J. Celmer, J. A. Koutcher, and R. R. Alfano, "UV reflectance spectroscopy probes DNA and protein changes in human breast tissues," J. Clin. Laser Med. Surg. **19,** 35–39 (2001).
7. N. Ghosh, S. K. Mohanty, S. K. Majumder, and P. K. Gupta, "Measurement of optical transport properties of normal and malignant human breast tissue," Appl. Opt. **40,** 176–184 (2001).
8. G. M. Palmer and N. Ramanujam, "Monte Carlo-based inverse model for calculating tissue optical properties. Part I: Theory and validation on synthetic phantoms," Appl. Opt. **45,** 1062–1071 (2006).
9. J. R. Mourant, J. P. Freyer, A. H. Hielscher, A. A. Eick, D. Shen, and T. M. Johnson, "Mechanisms of light scattering from biological cells relevant to noninvasive optical-tissue diagnostics," Appl. Opt. **37,** 3586–3593 (1998).
10. F. P. Bolin, C. R. Preuss, C. R. Taylor, and R. J. Ference, "Refractive index of some mammalian tissues using a fiber optic cladding method," Appl. Opt. **28,** 2297–2303 (1989).
11. F. A. Duck, *Physical Properties of Tissue: Comprehensive Reference Book* (Academic, 1990).
12. G. Zonios, L. T. Perelman, V. Backman, R. Manoharan, M. Fitzmaurice, J. Van-Dam, and M. S. Feld, "Diffuse reflectance spectroscopy of human adenomatous colon polyps *in vivo,*" Appl. Opt. **38,** 6628–6637 (1999).
13. J. R. Mourant, T. M. Johnson, and J. P. Freyer, "Characterizing mammalian cells and cell phantoms by polarized backscattering fiber-optic measurements," Appl. Opt. **40,** 5114–5123 (2001).
14. Y. Yang, E. J. Celmer, J. A. Koutcher, and R. R. Alfano, "DNA and protein changes caused by disease in human breast tissues probed by the Kubelka–Munk spectral functional," Photochem. Photobiol. **75,** 627–632 (2002).
15. S. Prahl, *Optical Properties Spectra* (Oregon Medical Laser Center, 2003); available at http://omlc.ogi.edu/spectra.
16. R. M. Bethea, B. S. Duran, and T. L. Boullion, *Statistical Methods for Engineers and Scientists* (Marcel Dekker, 1995).
17. S. Gunn, *Support Vector Machines for Classification and Regression* (University of Southampton, Department of Electronics and Computer Science, 1998); available at http://www.ecs.soton.ac.uk/~srg/publications/pdf/SVM.pdf.
18. C. Burges, "A tutorial on support vector machines for pattern recognition," Data Min. Knowl. Discov. **2,** 121–167 (1998).
19. P. I. Good, *Resampling Methods: A Practical Guide to Data Analysis* (Birkhäuser, 2001).
20. R. A. Johnson and D. W. Wichern, *Applied Multivariate Statistical Analysis* (Prentice-Hall, 2002).
21. C. Zhu, G. M. Palmer, T. M. Breslin, F. Xu, and N. Ramanujam, "Use of a multiseparation fiber optic probe for the optical diagnosis of breast cancer," J. Biomed. Opt. **10,** 024032-1–024032-13 (2005).
22. B. J. Tromberg, N. Shah, R. Lanning, A. Cerussi, J. Espinoza, T. Pham, L. Svaasand, and J. Butler, "Non-invasive *in vivo* characterization of breast tumors using photon migration spectroscopy," Neoplasia **2,** 26–40 (2000).
23. D. Grosenick, K. T. Moesta, H. Wabnitz, J. Mucke, C. Stroszczynski, R. Macdonald, P. M. Schlag, and H. Rinneberg, "Time-domain optical mammography: initial clinical results on detection and characterization of breast tumors," Appl. Opt. **42,** 3170–3186 (2003).
24. V. Chernomordik, D. W. Hattery, D. Grosenick, H. Wabnitz, H. Rinneberg, K. T. Moesta, P. M. Schlag, and A. Gandjbakhche, "Quantification of optical properties of a breast tumor using random walk theory," J. Biomed. Opt. **7,** 80–87 (2002).
25. S. Fantini, S. A. Walker, M. A. Franceschini, M. Kaschke, P. M. Schlag, and K. T. Moesta, "Assessment of the size, position, and optical properties of breast tumors *in vivo* by noninvasive optical methods," Appl. Opt. **37,** 1982–1989 (1998).
26. B. W. Pogue, S. P. Poplack, T. O. McBride, W. A. Wells, K. S. Osterman, U. L. Osterberg, and K. D. Paulsen, "Quantitative hemoglobin tomography with diffuse near-infrared spectroscopy: pilot results in the breast," Radiology **218,** 261–266 (2001).
27. D. Grosenick, H. Wabnitz, K. T. Moesta, J. Mucke, M. Moller, C. Stroszczynski, J. Stossel, B. Wassermann, P. M. Schlag, and H. Rinneberg, "Concentration and oxygen saturation of haemoglobin of 50 breast tumours determined by time-domain optical mammography," Phys. Med. Biol. **49,** 1165–1181 (2004).
28. S. Srinivasan, B. W. Pogue, S. Jiang, H. Dehghani, C. Kogel, S. Soho, J. J. Gibson, T. D. Tosteson, S. P. Poplack, and K. D. Paulsen, "Interpreting hemoglobin and water concentration, oxygen saturation, and scattering measured *in vivo* by near-infrared breast tomography," Proc. Natl. Acad. Sci. U.S.A. **100,** 12349–12354 (2003).